RSC Advances

PAPER

View Article Online
View Journal | View Issue

Cite this: *RSC Adv.*, 2023, **13**, 23267

Supramolecular assemblies in the molecular complexes of 4-cyanophenylboronic acid with different N-donor ligands †

Samina Easmin * and Venkateswara Rao Pedireddi

Molecular complexes of 4-cyanophenylboronic acid (**CB**) with various N-donor compounds having different conformational features, for example, rigid (1,10-phenanthroline (*110phen*), 4,7-phenanthroline (*47phen*), 1,7-phenanthroline (*17phen*) and acridine (*acr*)) and linear (1,2-bis(4-pyridyl)ethane (*bpyea*), 1,2-bis(4-pyridyl)ethene (*bpyee*) and 4,4′-azopyridine (*azopy*)), have been reported. In all complexes, the $-B(OH)_2$ moiety is found to be in a *syn–anti* confirmation, with the exception of structures containing *110phen*, *bpyee*, and *azopy*, wherein, *syn–syn* conformation is observed. Further, **CB** molecules remain intact in all structures except in the complexes with some linear N-donor ligands, wherein $-B(OH)_2$ transforms to monoester ($-B(OH)(OCH_3)$) prior to the formation of corresponding molecular complexes. In such boronic monoester complexes, the conformation of $-B(OH)(OCH_3)$ is *syn–anti* with respect to the $-OH$ and $-OCH_3$ groups. Also, complexes mediated by *azopy* and *bpyee* exist in both hydrated and anhydrous forms. In these anhydrous structures, the recognition pattern is through *homomeric* (juxtaposed $-CN$ and $-B(OH)_2$) as well as *heteromeric* (between hetero N-atom and $-B(OH)_2$) O–H···N hydrogen bonds, while only *heteromeric* O–H···N hydrogen bonds hold co-formers in all other structures. Depending upon the conformational features of both co-formers, molecules are packed in crystal lattices in the form of stacked layers, helical chains, and crossed ribbons. All structures are fully characterized by single-crystal X-ray diffraction and phase purity is established by powder X-ray diffraction. Additionally, correlation among structures is explained by calculating a similarity index and performing a Hirshfeld surface analysis to quantify the strength and effectiveness of different types of intermolecular bonds that stabilize these structures along with the presentation of energy frameworks, representing the strength of the interactions in the form gradient cylinders. Also, the morphology of each complex was computed by BFDH methodology to correlate with the actual crystal morphology and packing arrangement.

Received 12th June 2023
Accepted 17th July 2023

DOI: 10.1039/d3ra03936f

rsc.li/rsc-advances

1. Introduction

The design and preparation of new materials, for example, co-crystals, with desired physical and chemical properties is a continuum process.[1] The methodology involved in such experiments is essentially based on generating molecular recognition between the complementary molecular building blocks, invoking various intermolecular interactions such as hydrogen bonds, π–π interactions, *etc.*[2] However, since the intermolecular interactions are so labile and facile to either re-orient or reorganize, the development of target-oriented materials is still elusive, despite a plethora of structural assemblies known in the literature.[3]

Some functional groups like –COOH, $-CONH_2$, and $-CSNH_2$, form specific topological hydrogen bonding patterns that may determine the course of arrangement of molecules in crystal lattices; however, other auxiliary groups prevail on the molecules, and may also play a vital role in the ultimate topological arrangements.[4] In addition, if the prime functional group shows high conformational flexibility to form distinct conformers, the degree of molecular aggregation further would expand and accordingly a diversity of archetypes may form.[4c,5] Among such functional groups, an organoboronic acid, represented as $-B(OH)_2$, shows three conformers in solid-state that can produce diverse recognition patterns, *syn–anti*, *syn–syn*, and *anti–anti*, as shown in Scheme 1, possibly leading to the formation more intriguing exotic supramolecular architectures.[6]

Organoboronic acids are an important and significant class of compounds that have gained prominence due to their

Solid State and Supramolecular Chemistry Laboratory, School of Basic Sciences, Indian Institute of Technology Bhubaneswar, Argul, Bhubaneswar 752 050, India. E-mail: se15@iitbbs.ac.in

† Electronic supplementary information (ESI) available: ORTEP plots, powder X-ray diffraction patterns, packing analysis, isostructurality, Hirshfeld surface analysis and interaction energy. CCDC 2260224, 2260225, 2260226, 2260227, 2260231, 2260232, 2260233, 2260234, 2260235, 2260236 and 2260237. For ESI and crystallographic data in CIF or other electronic format see DOI: https://doi.org/10.1039/d3ra03936f

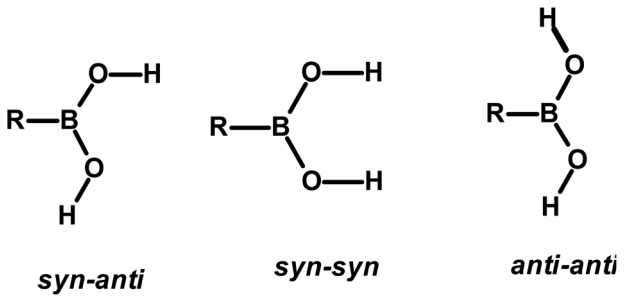

Scheme 1

applications in organic synthesis, mainly in Suzuki coupling reaction[7] and medicinal chemistry like enzyme inhibitors,[8] saccharide, sensing agents,[9] boron neutron capture therapy agents, *etc.*[10] In fact, a recently emerging novel frontier research area, covalent organic frameworks (COFs), is also mainly due to the facile reactive features of boronic acids to form C–C bonds with ease in the presence of appropriate organic ligands.[11] Apart from it, boronic acids have recently gained popularity in supramolecular chemistry due to the potency of $-B(OH)_2$ moiety as a hydrogen bond donor as well as an acceptor, similar to carboxylic acid and amide functionalities.[6a,12]

Despite the demonstrated capability of the $-B(OH)_2$ moiety to form O–H···O/O–H···N hydrogen bonds with various co-formers, similar to –COOH and $-CONH_2$ groups, the number of structural investigations involving boronic acids is still significantly lower compared to carboxylic acid and amide complexes.[3b,13]

Thus, considering the significance of boronic acids in the general synthetic aspects and also effective applications in healthcare domains, as well as the most significant feature of the facile formation of different hydrogen bonding patterns and considerably a small number of studies only are available in the literature, different exercises have been carried out to develop a myriad of boronic acids in the form co-crystals.[14]

In this regard, an important feature derived from the literature is that 4-cyanophenylboronic acid (**CB**) is known to form only hydrated molecular complexes with some linear N-donor ligands, despite water is not used as a crystallization solvent.[15] Thus, several co-crystallization experiments have been initiated to develop corresponding anhydrous complexes of **CB** and also by expanding the horizon of N-donors by considering rigid ligands as well, by employing 1,10-phenanthroline (*110phen*), 4,7-phenanthroline (*47phen*), 1,7-phenanthroline (*17phen*), acridine (*acr*) and 4,4′-azopyridine (*azopy*), 1,2-bis(4-pyridyl)ethane (*bpyea*) and 1,2-bis(4-pyridyl)ethene (*bpyee*). The three-dimensional structures of all co-crystals, thus, obtained have been determined by single crystal X-ray diffraction method to evaluate the exotic structural features. The asymmetric unit contents of each complex are presented (Table S1) in the form of ORTEP in the ESI.†

2. Experimental section

The chemicals used in this study were obtained from Sigma-Aldrich with >99% purity and have been used without further purification. The solvents employed for crystallization experiments were of the highest quality available (spectroscopy grade). The co-crystals were prepared by dissolving the corresponding reactants in an appropriate solvent and allowing the solution to evaporate either at ambient or low-temperature conditions. Within 72–96 hours, good-quality single crystals suitable for X-ray diffraction analysis were obtained in all instances.

2.1. Crystal structure determination

Good-quality single crystals were carefully chosen after being viewed under a Leica microscope and glued to glass fiber by using an adhesive, and mounted on the goniometer of Bruker single-crystal X-ray diffractometer (D8 VENTURE), with Mo-Kα radiation ($\lambda = 0.71073$ Å) source, equipped with a PHOTON 100 CMOS detector. The crystals remained stable throughout the data collection, carried out in φ and ω scans, and the process was found to be smooth. The structures were determined by using the intrinsic phasing method followed by full-matrix least-squares refinement against F^2 using SHELXTL, embedded within Bruker suite of programs.[16] All non-hydrogen atoms were refined by anisotropic method and hydrogen atoms were either refined or placed in calculated positions (Table S2†). All the structural refinements converged to good R factors, as listed in Table 1 and the intermolecular interactions were computed by using PLATON (see Table 2).[17] The packing diagrams were generated by using Diamond (version 4.6.3).[18]

2.2. Powder X-ray diffraction (PXRD)

PXRD patterns were recorded on a Bruker D8 Advance X-ray diffractometer with Cu-Kα radiation ($\lambda = 1.5418$ Å). The voltage and current applied were 40 kV and 30 mA, respectively. Intensities were measured in the reflection mode in the 2θ range of 5–40°.

2.3. Hirshfeld surface analysis

Hirshfeld surface analysis and 2D fingerprint calculations were performed using Crystal Explorer (*version 21*),[19] by importing the atomic coordinates from the CIF files. Hirshfeld surfaces (separately for each co-former) are generated for each structure. The distance from the nearest nucleus inside and outside the surface was measured and represented by the d_i and d_e, respectively, while a normalized contact distance was represented as d_{norm}. The white, red, and blue colors have been selected for the visualization of the d_{norm} function with very high resolution.

2.4. Energy framework

The energy frameworks for all the co-crystals have been estimated based on the interaction energies by using Crystal Explorer 21.5 software.[19] The energy calculations are performed at the B3LYP/6-31G(d,p) level of theory and using the crystal geometry of the respective co-crystals. The energy framework was constructed with an equal tube size (scale factor) of 100 and the energy threshold (cut-off) value was set to 5 kJ mol^{-1}.

Table 1 Crystallographic data for the molecular complexes, **1–7**, **6a**, **6b**, **7a** and **7b**

Parameters	**1**	**2**	**3**	**4**	**5**	**6**	**6a**	**6b**	**7**	**7a**	**7b**
Formula	$(C_{12}H_8N_2)$: $(C_7H_6BNO_2)$: (CH_3OH)	$(C_{12}H_8N_2)$: $(C_7H_6BNO_2)$	$(C_{12}H_8N_2)$: $(C_7H_6BNO_2)$	$(C_{13}H_9N)$: $(C_7H_6BNO_2)$	$(C_7H_6BNO_2)$: $(C_{12}H_{12}N_2)$: (H_2O)	$2(C_7H_6BNO_2)$: $(C_{10}H_8N_4)$	$(C_{10}H_8N_4)$: $(C_7H_6BNO_2)$: (H_2O)	$2(C_8H_8BNO_2)$: $(C_{10}H_8N_4)$	$2(C_7H_6BNO_2)$: $(C_{12}H_{10}N_2)$	$2(C_7H_6BNO_2)$: $(C_{12}H_{10}N_2)$: 4(O)	$2(C_8H_8BNO_2)$: $(C_{12}H_{10}N_2)$
M_r	355.15	327.14	327.14	326.15	349.19	478.08	349.16	506.13	476.09	524.65	504.15
Crystal color	Colorless	Brown	Brown	Yellow	Colorless	Orange	Orange	Orange	Colorless	Colorless	Colorless
Crystal shape	Needle	Needle	Plate	Block	Blade	Plate	Block	Needle	Plate	Needle	Needle
T/K	293(2)	293(2)	293(2)	293(2)	293(2)	293(2)	293(2)	293(2)	293(2)	293(2)	293(2)
λ(Mo-K$_\alpha$)/Å	0.71073	0.71073	0.71073	0.71073	0.71073	0.71073	0.71073 Å	0.71073	0.71073	0.71073	0.71073
Crystal system	Orthorhombic	Monoclinic	Triclinic	Monoclinic	Triclinic	Monoclinic	Triclinic	Monoclinic	Monoclinic	Triclinic	Monoclinic
Space group	$P2_12_12_1$	$P2_1$	$P\bar{1}$	$P2_1/n$	$P\bar{1}$	$P2_1/c$	$P\bar{1}$	$P2_1/c$	$P2_1/c$	$P\bar{1}$	$P2_1/c$
a/Å	3.8278(3)	14.8728(7)	7.1497(3)	11.0840(8)	7.5470(4)	8.2777(5)	8.8653(3)	3.8043(3)	8.4431(5)	3.8665(2)	3.9427(2)
b/Å	17.1899(6)	3.8786(2)	8.7492(4)	7.3311(5)	11.5173(7)	7.1087(4)	9.0872(4)	22.3944(13)	7.3205(4)	11.5022(5)	22.6930(9)
c/Å	26.2562(9)	15.4857(8)	13.6709(6)	21.0913(13)	11.9183(8)	19.6723(9)	12.2227(6)	14.7329(8)	19.6867(9)	15.8177(8)	14.9291(6)
α/°	90	90	97.158(4)	90	99.982(5)	90	105.549(4)	90	90	77.285(2)	90
β/°	90	115.182(5)	96.960(3)	99.007(6)	102.829(4)	95.218(2)	108.761(5)	94.107(6)	93.592(4)	86.962(4)	93.421(7)
γ/°	90	90	95.413(4)	90	105.296(7)	90	90.865(7)	90	90	87.577(5)	90
V/Å^3	1727.64(16)	808.40(8)	837.04(6)	1692.7(2)	944.22(11)	1152.79(11)	892.67(7)	1251.95(14)	1214.40(11)	684.91(6)	1333.35(10)
Z	4	2	2	4	2	2	2	2	2	1	2
D_c/g cm^{-3}	1.365	1.344	1.298	1.280	1.228	1.377	1.299	1.343	1.302	1.272	1.256
μ/mm^{-1}	0.093	0.088	0.085	0.083	0.083	0.095	0.091	0.092	0.088	0.092	0.084
F(000)	736	340	340	680	368	496	364	528	496	274	528
θ range [°]	1.95–26.65	2.50–26.33	2.36–26.58	2.23–26.37	1.80–26.67	3.04–26.42	2.34–26.54	3.31–26.38	2.07–26.34	1.99–26.62	2.25–26.45
Index ranges	$-4 \le h \le 4$ $-21 \le k \le 21$ $-33 \le l \le 33$	$-18 \le h \le 17$ $-4 \le k \le 4$ $-15 \le l \le 19$	$-8 \le h \le 7$ $-11 \le k \le 10$ $-17 \le l \le 17$	$-13 \le h \le 13$ $-9 \le k \le 9$ $-20 \le l \le 26$	$-9 \le h \le 9$ $-14 \le k \le 14$ $-15 \le l \le 14$	$-9 \le h \le 10$ $-8 \le k \le 7$ $-22 \le l \le 24$	$-11 \le h \le 11$ $-11 \le k \le 11$ $-15 \le l \le 15$	$-4 \le h \le 4$ $-27 \le k \le 23$ $-18 \le l \le 18$	$-10 \le h \le 10$ $-9 \le k \le 9$ $-24 \le l \le 24$	$-4 \le h \le 4$ $-12 \le k \le 14$ $-19 \le l \le 19$	$-4 \le h \le 4$ $-28 \le k \le 28$ $-18 \le l \le 13$
Reflections	39 424	8701	14 761	11 943	26 286	6771	25 898	9656	14 399	14 656	9015
Unique reflections	3595	3256	3431	3443	3941	2350	3672	2540	2462	2779	2719
No. of parameters	250	228	229	229	265	177	261	175	178	182	185
GooF on F^2	1.009	1.007	1.004	1.007	1.001	1.005	1.008	1.006	1.002	1.008	1.002
R_1, $[I > 2\sigma(I)]$	0.053	0.057	0.055	0.051	0.064	0.045	0.055	0.058	0.046	0.073	0.060
wR_2, $[I > 2\sigma(I)]$	0.125	0.139	0.138	0.117	0.165	0.113	0.1427	0.141	0.105	0.1975	0.137
Largest diff. peak and hole (e Å^{-3})	0.34/−0.38	0.18/−0.19	0.17/−0.14	0.19/−0.17	0.18/−0.18	0.29/−0.35	0.19/-0.25	0.35/−0.25	0.12/−0.15	0.32/−0.20	0.17/−0.16
CCDC No.	2260224	2260226	2260225	2260227	2260237	2260231	2260236	2260234	2260235	2260233	2260232

Table 2 Hydrogen bond distances (Å) and angles (°) for all molecular complexes, **1–7**, **6a**, **6b**, **7a** and **7b**[a]

Co-crystals	O–H···O			O–H···N			C–H···O			C–H···N		
1				1.79	2.74(2)	163	2.46	3.52(2)	169	2.67	3.50(2)	134
				1.81	2.79(2)	172	2.88	3.87(2)	152	2.75	3.54(2)	130
							2.54	3.60(2)	168			
2				1.85	2.79(1)	158	2.39	3.43(3)	164	2.54	3.59(2)	164
				1.98	2.88(2)	151	2.53	3.58(1)	162	2.56	3.51(1)	147
										2.63	3.69(2)	164
3	1.81	2.78(3)	171	1.84	2.72(3)	148	2.32	3.3(3)	153	2.58	3.58(1)	153
										2.59	3.58(2)	151
										2.73	3.70(1)	149
4	1.78	2.75(2)	169	1.80	2.69(2)	149	2.42	3.45(3)	160	2.47	3.46(3)	152
							2.86	3.76(3)	141			
5	1.77	2.68(2)	153	1.78	2.75(2)	172	2.65	3.46(3)	132			
				1.88	2.79(2)	154	2.70	3.52(3)	133			
				2.03	2.94(2)	155	2.90	3.76(3)	138			
6				1.87	2.76(3)	150	2.63	3.47(2)	134	2.52	3.49(3)	148
				1.98	2.91(3)	157	2.81	3.77(3)	148	2.84	3.71(1)	138
6a	1.97	2.72(1)	131	1.81	2.77(3)	164	2.49	3.45(3)	149	2.45	3.51(3)	167
	1.84	2.72(1)	148	1.87	2.79(2)	156	2.83	3.67(2)	134	2.71	3.67(2)	148
6b				1.87	2.75(2)	148	2.42	3.47(3)	163	2.56	3.47(3)	141
										2.92	3.84(3)	143
										2.64	3.59(3)	148
7				1.85	2.74(3)	149	2.94	3.86(3)	143	2.56	3.52(3)	149
				2.01	2.96(3)	162				2.76	3.68(3)	143
7a	1.81	2.77(3)	168	1.79	2.71(3)	154	2.36	3.41(3)	165	2.36	3.41(3)	165
	1.83	2.71(3)	148				2.48	3.51(3)	158	2.62	3.65(3)	158
	1.84	2.71(3)	147							2.79	3.77(3)	151
										2.82	3.71(3)	140
7b				1.87	2.74(2)	147	2.71	3.74(2)	160	2.64	2.60(2)	148
										2.70	3.52(2)	133

[a] For each structure, the three columns represent the distances of H···A, D···A and angles ∠D–H···A, respectively.

3. Results and discussion

Good-quality single crystals of **CB** with various N-donor compounds as listed in Chart 1 are obtained upon co-crystallization from an appropriate solvent (Chart 1). Structure determination of these complexes reveals that each adduct forms distinctly unique molecular arrangements, especially the conformation of $-B(OH)_2$ moiety and the nature of hydrogen bonds (*homomeric* and *heteromeric*), which are discussed in detail for all complexes.

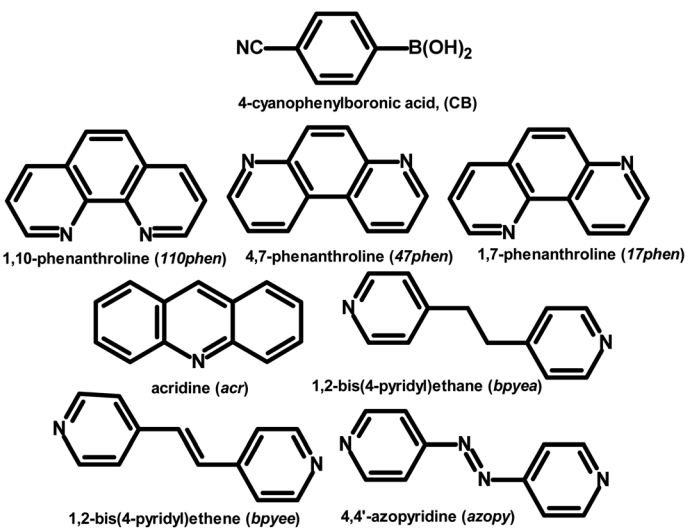

Reactants	solvents	products
CB + *110phen*	CH_3OH	**1**
CB + *47phen*	CH_3OH	**2**
CB + *17phen*	CH_3OH	**3**
CB + *acr*	CH_3OH	**4**
CB + *bpyea*	CH_3OH	**5**
CB + *azopy*	CH_3NO_2	**6**
	CH_3OH	**6a & 6b**
CB + *bpyee*	CH_3CN	**7**
	C_2H_5OH	**7a**
	CH_3OH	**7b**

Chart 1

3.1. Molecular complexes of CB with rigid N-donor ligands

Molecular complex of CB with *110phen*. At ambient conditions, co-crystallization of 4-cyanophenylboronic acid, **CB**, with *110phen*, from a CH_3OH solution of the co-formers in a 1 : 1 ratio, gives needle-shaped good-quality single crystals within 72 h, which are labeled as **1** for ease of discussion. X-ray diffraction analysis reveals that the components of **1**, crystallize in an orthorhombic non-centrosymmetric (chiral) $P2_12_12_1$ space group, with an asymmetric unit consisting of 1 : 1 molecule of co-formers and molecules of crystallization solvent (CH_3OH). The pertinent crystallographic information is given in Table 1. The constituents of an asymmetric unit are shown in Table S1,† in the form of ORTEP.

The molecules in complex **1** arrange in the form of sheets with voids (7 × 6 Å^2) that are inhabited by molecules of crystallization solvent (CH_3OH), as shown in Fig. 1a. The guest molecules (CH_3OH), indeed, form infinite chains by holding each other through hydrogen bonds. Within each sheet, the co-formers interact with each other through O–H···N hydrogen bonds formed between $-B(OH)_2$ moiety prevails on **CB** and the N-atoms of *110phen*. It is pertinent to mention that such a recognition process involves $-B(OH)_2$ moiety in a *syn–syn* conformation, which is a commonly known conformation in similar complexes.[6d,20] The hydrogen bonds, thus, formed appear in the form of an unsymmetrical Etter's pattern, $R_2^2(9)$, with the corresponding H···N distances being 1.79 Å (O···N, 2.74 Å) and 1.81 Å (O···N, 2.79 Å) as shown in Fig. 1b. Furthermore, the assemblages self-assemble to constitute quartet ensembles through the formation of C–H···O (H···O, 2.46 Å; C···O, 3.52 Å) hydrogen bonds (*homomeric*, between the molecules of **CB**) in the form of a symmetrical pattern, $R_2^2(12)$ and a single C–H···N (*heteromeric*, between the co-formers) hydrogen bond, with the corresponding H···N distance being 2.75 Å (C···N, 3.54 Å). In turn, these quartets are held together by different C–H···O and C–H···N hydrogen bonds with H···O, 2.54 Å, (C···O, 3.60 Å) and H···N, 2.67 Å, (C···N, 3.54 Å) respectively. However, in the crystal lattice, the sheets are not stacked translationally but are arranged in a crossed-sheet form. As a result, the juxtaposed molecules in the adjacent sheets interact with each other *via* the formation of helical chains among the molecules of **CB** (Fig. 1c). Further, the helical chains are bound together by the *110phen* molecules (Fig. 1d).

Molecular complex (2) of CB with *47phen*. A CH_3OH solution containing boronic acid, **CB** and *47phen* in a 1 : 1 ratio, upon slow evaporation, forms needle-shaped crystals at ambient conditions. The molecules in the crystals are arranged in a monoclinic non-centrosymmetric space group $P2_1$, with an asymmetric unit consisting of co-formers in a 1 : 1 molecular ratio (Table S1†). Unlike in the crystals of **1**, herein, $-B(OH)_2$ moiety is found in a *syn–anti* conformation.

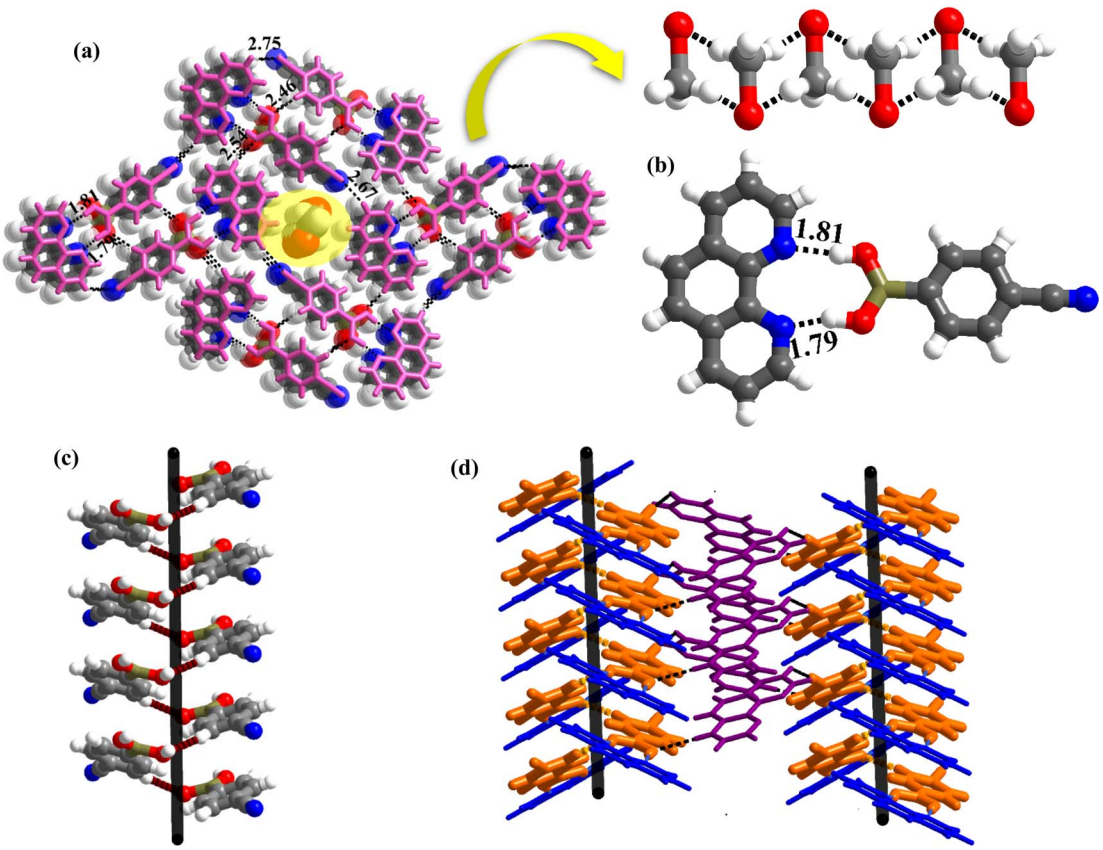

Fig. 1 (a) Three-dimensional arrangement with voids, occupied by CH_3OH molecules, in molecular complex, **1**. (b) Basic recognition unit observed between complementary functional groups present in **1**. (c) 1D helical chain and (d) left-handed and right-handed helical chains.

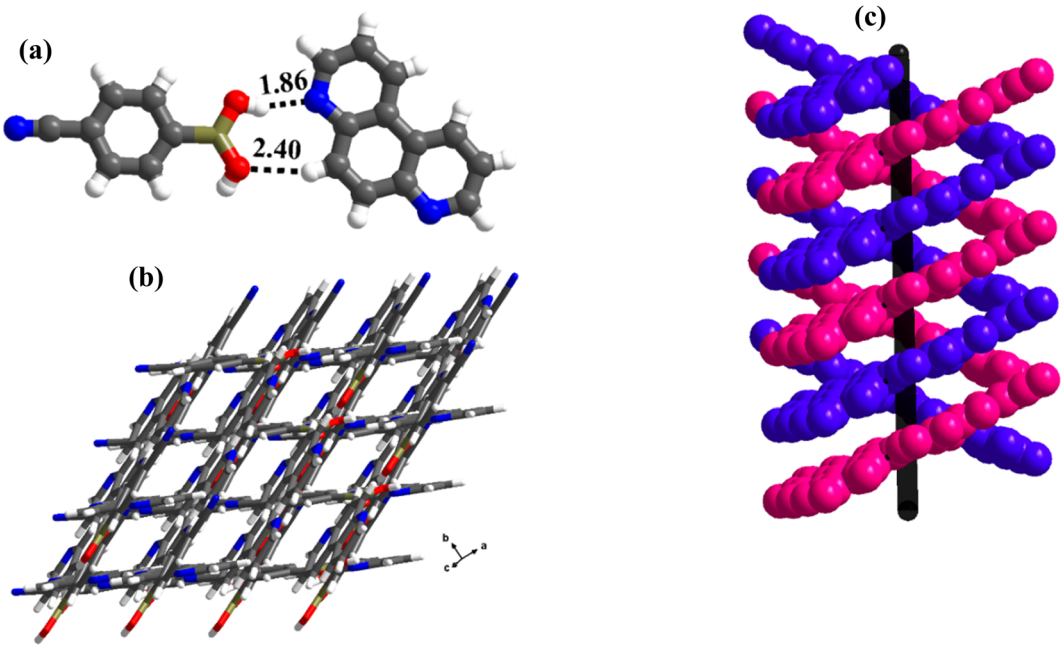

Fig. 2 (a) Basic recognition unit observed in molecular complex, **2**. (b) Criss-crossed network in the crystal lattice. (c) A double helix formed between **CB** and *47phen*.

Structural analysis shows that the building unit between **CB** and *47phen* molecules in this complex is formed through a *heteromeric* pairwise O–H···N/C–H···O (H···N, 1.85 Å; O···N, 2.79 Å and H···O, 2.39 Å; C···O, 3.43 Å) hydrogen bonds in the form of Etter's notation, $R_2^2(8)$ (Fig. 2a), and yields a crisscrossed network in the crystal lattice (Fig. 2b). Further, the adjacent building units are bound together by an O–H···N (H···N, 1.98 Å; O···N, 2.88 Å) hydrogen bond formed between *47phen* and **CB** molecules, invoking H-atom prevail on **CB** at the *anti*-position. Such an association, thereby, constitutes one-dimensional helical chains that are further held together by C–H···N (H···N, 2.54 Å; C···O, 3.59 Å) hydrogen bonds (Fig. 2c), leading to the construction of a double helix pattern.

Mimicking a recognition pattern of an amide functionality by –B(OH)$_2$ in molecular complex 3. Co-crystallization of **CB** with *17phen* (in a 1 : 1 ratio) forms crystals, **3**, at ambient conditions, during slow-evaporation of a CH_3OH solution of the co-formers. Structure determination by single-crystal X-ray diffraction method on a good-quality crystal reveals that the co-formers in the crystals of **3** crystallize in a triclinic space group, $P\bar{1}$, with an asymmetric unit consisting of molecules of **CB** and *17phen* in a 1 : 1 ratio (Table S1†).

Similar to **2**, here also the –B(OH)$_2$ moiety of **CB** espouses a *syn–anti* conformation, with unprecedented interactions with the co-former, *17phen*. In general, –B(OH)$_2$ has been addressed as a hybrid of –COOH and –CONH$_2$ based on the *homomeric* interactions in the native structures of several boronic acids, but it mostly mimics molecular recognition features of –COOH in many complexes, though a few recognition patterns of amides are also realized.[21] However, a significant pattern observed in amide-mediated co-crystals, for example, dimers of –CONH$_2$ moieties holding the co-formers through the second –

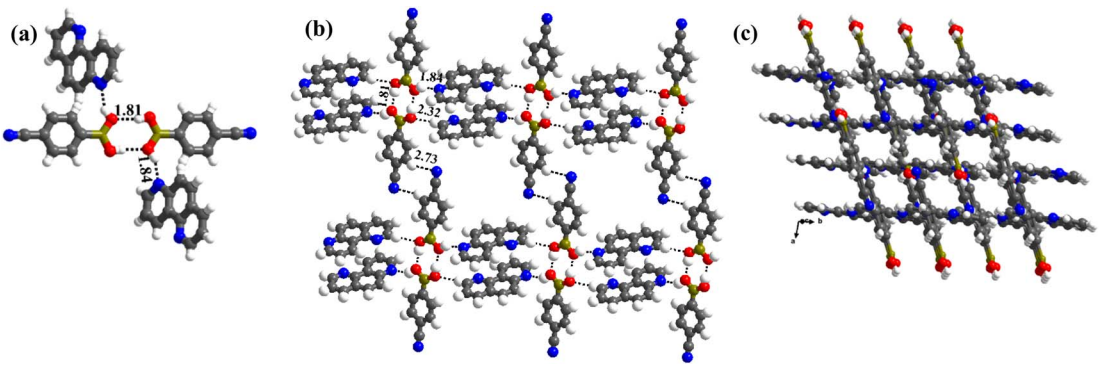

Fig. 3 (a) A typical tetrameric unit in the crystal structure of **3**. (b) Interaction between the tetramers in the crystal lattice. (c) Crossed tape networks in molecular complex, **3**.

NH group, is not so observed in the complexes of boronic acids (see Scheme S1†).[22]

In complex, **3**, interestingly, such an unusual amide feature is observed, for the first time, among boronic acid molecular complexes. Thus, molecules of **CB** form dimers through *homomeric* O–H···O (H···O, 1.81 Å; O···O, 2.78 Å) hydrogen bonds formed between the $-B(OH)_2$, in the form of centrosymmetric $R_2^2(8)$ pattern. Additionally, other H-atoms on both paired molecules establish interaction with *17phen* molecules *via heteromeric* O–H···N (H···N, 1.84 Å; O···N, 2.72 Å) hydrogen bonds, thus, creating tetrameric units (Fig. 3a). These units are further held together by C–H···O (H···O, 2.32 Å; O···N, 3.30 Å) hydrogen bonds, as shown in Fig. 3b. Nonetheless, the arrangement constitutes crossed tape networks in the crystal lattice, which are stabilized by *homomeric* C–H···N (H···N, 2.73 Å; C···N, 3.70 Å), hydrogen bonds (Fig. 3c).

Molecular recognition features and packing of molecules in co-crystals, 4 (CB with *acr*). A CH_3OH solution of **CB** and *acr*, upon slow evaporation at ambient temperature, gives good-quality single crystals. For ease of discussion, the crystals are labeled as **4**. The structure of **4**, determined by X-ray diffraction methods discloses that **4**, crystallizes in a monoclinic space group $P2_1/c$, with an asymmetric unit consisting of co-formers in a 1 : 1 molecular ratio. The constituents of an asymmetric unit are displayed in the form of ORTEP (Table S1†).

Conformation of $-B(OH)_2$ in this complex is also in the form of *syn–anti* as observed in **2** and **3**. Furthermore, the basic recognition patterns with the co-former reflect the amide pattern, the same as found in complex **3**. Thus, **CB** molecules interact with each other, yielding *homomeric* dimers in a centrosymmetric O–H···O (H···O, 1.78 Å; O···O, 2.75 Å) hydrogen bonding pattern, as shown in Fig. 4a. These dimers further form a tetrameric unit by interacting with *acr* molecules through *heteromeric* O–H···N (H···N, 1.80 Å; O···N, 2.69 Å) hydrogen bond, as shown in Fig. 4a. In such a pattern, though *acr* molecules appear to be like hanging pendants connected to a chain of **CB** molecules, in further self-assembly, *acr* molecules are connected to adjacent tetramers by C–H···O (H···O, 2.42 Å; C···O, 3.45 Å) hydrogen bonds formed between aromatic –CH groups on *acr* and –O atom of $-B(OH)_2$ moiety (Fig. 4a). Such aggregates are held together as crinkle chains in the crystal lattice by C–H···N (H···N, 2.47 Å; C···N, 3.46 Å) hydrogen bond, as depicted in Fig. 4 (*acr* molecules are not shown for brevity purposes). Complete details of all the pertinent hydrogen bond distances are given in Table 2.

The structural features of complexes **1–4**, show clear variations due to the diverse conformations of $-B(OH)_2$ influenced by N-atom locations on aza-donors. For example, *110phen*, having juxtaposed N-atoms directs to have a *syn–syn* conformation in **CB** molecules, while widely separated N-atoms mediated *17phen*, induces *syn–anti* conformations in **CB** molecules, as also observed in the literature even with linear ligands like 4,4′-bipyridine (*bpy*) and *bpyee*.

3.2. Molecular complexes of CB with linear N-donor ligands

In the literature, **CB** molecular complexes with linear ligands (*bpy* and *bpyee*), are noted to be hydrated only. Also, co-crystals of **CB** with *bpyea* and *azopy* (higher homologous of *bpy* and analogous to *bpyee*) are not yet reported in the literature. Hence, co-crystallization of **CB** with *bpyea* and *azopy* has been carried out and the derived structural features are illustrated below.

Stacked sheet structure in the molecular complex 5 (CB and *bpyea*). Crystals of complex **5** are obtained through a co-crystallization experiment by dissolving 1 : 1 ratio **CB** and *bpyea* co-formers in CH_3OH and subsequently evaporating the solution slowly at ambient conditions. Though water is not used in the crystallization process, the asymmetric unit is noted to be associated with a water molecule also, which is in accordance with the nature of acid **CB** as is known to form hydrated complexes.[15] In fact, the structure analysis by single-crystal X-ray diffraction method, further discloses that complex **5** is isomorphous to the molecular complex formed by its analog, *bpyee*, which also gives a monohydrated molecular complex while crystallizing from a CH_3OH solution. The contents of the asymmetric unit are shown in Table S1,† representing water molecules also, in the form of ORTEP.

The analysis further discloses that the $-B(OH)_2$ moiety is present in *syn–anti* conformation as observed in **2–4**. In addition, the co-formers are arranged in a stacked sheets form in the crystal lattice as shown in Fig. 5a, with each sheet comprising both co-formers. The co-formers within each sheet are held

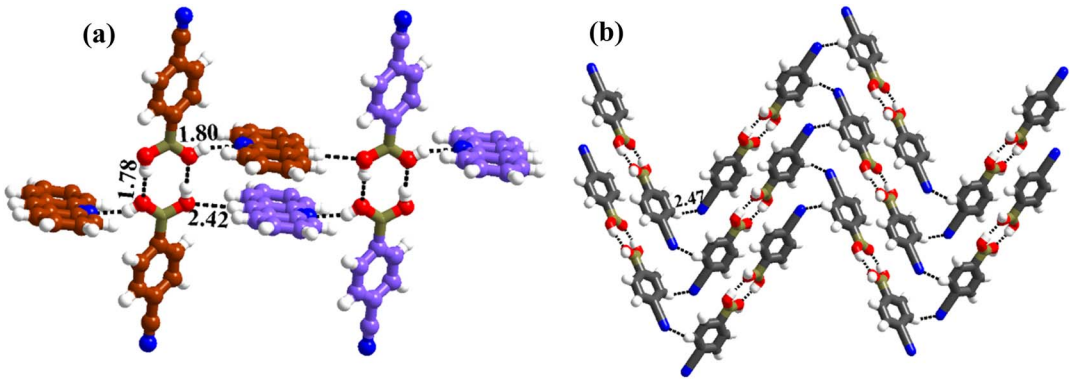

Fig. 4 (a) Basic interaction in the form of a tetramer and between the adjacent tetramers in complex, **4**. (b) Crinkle arrangement of **CB** molecules through C–H···N hydrogen bonds.

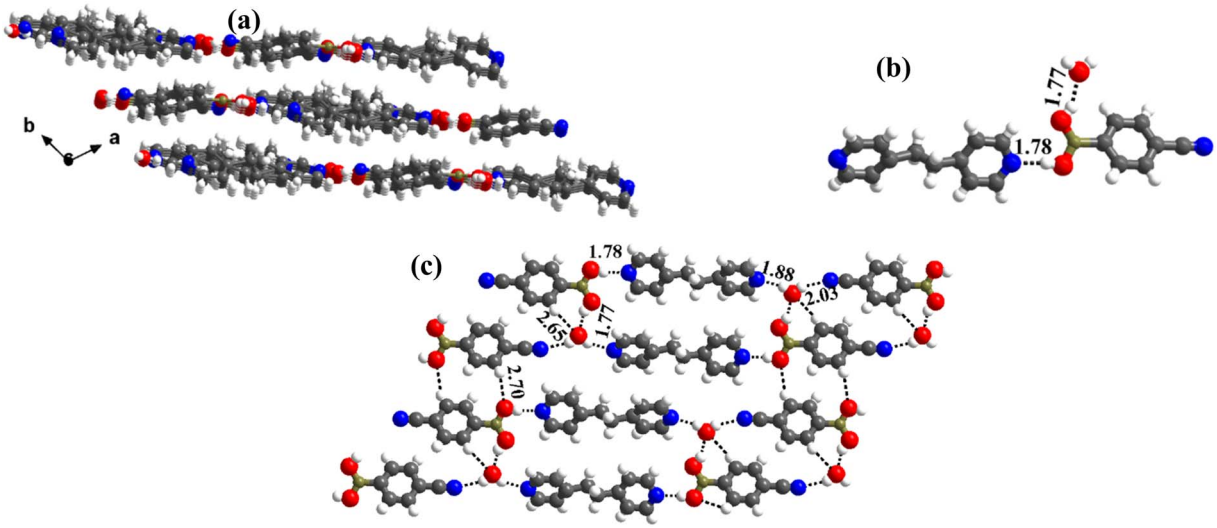

Fig. 5 (a) Sheet arrangement of the molecules in the crystal lattice. (b) Basic recognition of **CB** with *bpyea* in hydrated complex **5**. (c) Two-dimensional linear ribbon arrangement.

together by O–H···N (H···N, 1.78 Å; O···N, 2.72 Å) hydrogen bonds between –N atom of *bpyea* and $-B(OH)_2$ moiety, as also observed in the other structures discussed above, and are further connected through water molecules (see Fig. 5b). Thus, linear ribbons are formed in a one-dimensional arrangement with the adjacent primary blocks connected by two O–H···N (H···N, 1.88 and 2.03 Å; O···N, 2.79 and O···N, 2.94 Å) hydrogen bonds formed between water and –N atoms of *bpyea* and nitrile (–CN) groups. Such linear ribbons are further held together by O–H···O (H···O, 1.77 Å; O···O, 2.68 Å) hydrogen bonds formed by water molecules with $-B(OH)_2$ moiety as well as by some C–H···O hydrogen bonds with aza-donor molecules, as vividly shown in Fig. 5c.

Anhydrous molecular complex of CB with *azopy* in the crystal 6. Co-crystallization of *azopy* and **CB** from CH_3NO_2 gives good-quality homogenous single-crystals; nevertheless, the same co-formers yield two distinct morphological crystals (needle and block), concomitantly, from a CH_3OH solution. The structural details of each crystal are described as given below.

The structure analysis reveals that the co-crystals of *azopy* and **CB**, obtained from CH_3NO_2 (labeled as **6**), crystallize in a monoclinic space group, $P2_1/c$, with unit cell dimensions, as presented in Table 1. The contents of the asymmetric unit as depicted in Table S1,† reveals that structure **6** is an anhydrous complex of **CB** and *azopy* in a 2 : 1 ratio.

The analysis of molecular features of co-formers in **6** exposes that $-B(OH)_2$ moiety is in unusual *syn–syn* conformation, as observed in complex **1**, despite the absence of juxtaposed –N atoms on aza-donor molecules, expressing the two –OH groups of $-B(OH)_2$ moiety as vicinal diols. In fact, the observed conformation is quite intriguing and certainly accounted for the molecular recognition process between the co-former molecules **CB** and *azopy*. Further, the azo-bridge (–N=N) in *azopy* molecules is noted to be disordered in a 2 : 1 ratio. Thus, the co-formers are held together by *heteromeric* O–H···N (H···N, 1.87 Å; O···N, 2.76 Å) hydrogen bonds between molecules of **CB** and *azopy*; however, an unusual *homomeric* O–H···N (H···N, 1.98 Å; O···N, 2.91 Å) hydrogen bond is also observed, which is formed between **CB** molecules (formed between $-B(OH)_2$ and nitrile group), a hitherto unknown pattern in any of the **CB** complexes. The pattern (both *homomeric* and *heteromeric*), along with its propagation is shown in Fig. 6a. Such an association further

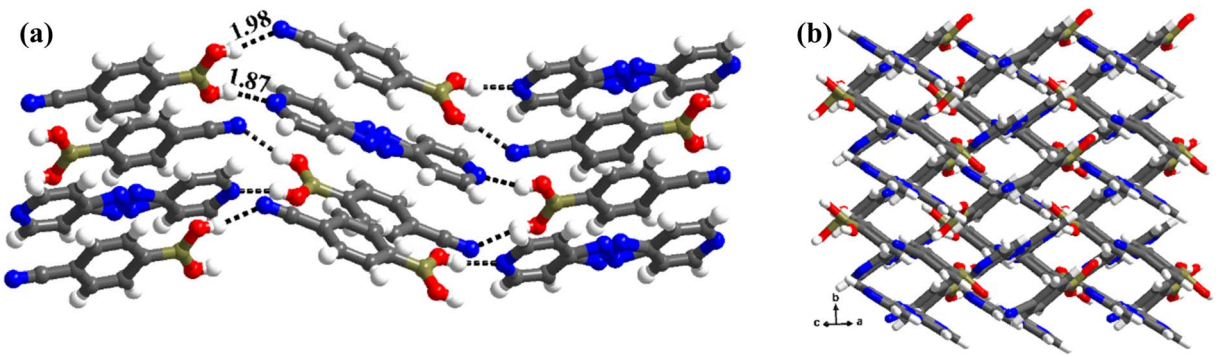

Fig. 6 (a) Propagation of chain arrangement in the molecular complex, **6**. (b) Crossed ribbon arrangement present in the crystal lattice.

leads to the formation of crossed ribbon structures, as shown in Fig. 6b.

Concomitant crystals (block and needle-shaped) of CB and *azopy* from CH_3OH. Single crystal X-ray diffraction reveals that out of the two concomitant crystals (block and needle-shaped) obtained from CH_3OH (mentioned in the text earlier), block-shaped crystals are noted to be a hydrated form of **CB** and *azopy* (labeled as **6a**), as same as the complex of **CB** with *bpyee* that was already reported in the literature (CSD refcode: **PELMUR**).[15] The detailed analysis further reveals that **6a** also crystallizes in a triclinic $P\bar{1}$ space group, with an asymmetric unit having 1 : 1 molecules of co-formers and a water molecule. The constituents of the asymmetric unit are shown in Table S1.† Crystals of **6a** (see Table 1) are found to be isomorphous with **PELMUR** (a = 8.918(2), b = 9.508(2), c = 12.009(3) Å and α = 71.75(1), β = 70.21(1), γ = 89.23(1)°). Also, **6a** and **PELMUR** show an isostructural relationship, despite the $-B(OH)_2$ moiety present in different conformations (*syn–syn*, **6a**; *syn–anti*, **PELMUR**). The structural features of **6a** are described below.

The needle-shaped crystals, however, on the other hand interestingly have shown entirely a new feature with the formation of co-crystals generated between *in situ* converted monoester of **CB** and *azopy*. These crystals are labeled **6b** and the structural features are discussed in detail in later sections.

Stacked layer structure in crystal structure of complex, 6a. Crystals of **6a**, with the contents of **CB** and *azopy* in a 1 : 1 ratio along with a water molecule also, form a stacked layers structure in a three-dimensional arrangement (along *a*-axis), as shown in Fig. 7a. In such an arrangement, the $-B(OH)_2$ moiety, in a *syn–syn* confirmation, establishes interaction through O–H···N (H···N, 1.81 and 1.87 Å; O···N, 2.77 and 2.79 Å) and O–H···O (H···O, 1.97 Å; O···O, 2.72 Å) hydrogen bonds, directly with N-atom of *azopy* and with the aid of water molecules, respectively. Thus, a cyclic six molecular unit (two of each **CB**, *azopy* and H_2O) is realized, as pictorially depicted in Fig. 7b. The cyclic units (highlighted in Fig. 7c) are further held together in a two-dimensional arrangement by establishing a centrosymmetric *homomeric* C–H···N (H···N, 2.71 Å; C···N, 3.67 Å) hydrogen bonding mediated $R_2^2(10)$ pattern between the adjacent **CB** molecules (see Fig. 7c).

It is well documented in the literature that hydrates and anhydrous forms of the same co-formers are generally prepared by varying the crystallization conditions, such as solvents, temperature, pH, *etc.*[23] Incidentally, by altering the solvent of crystallization, *azopy* has been noted to form both anhydrous and hydrated complexes **6** and **6a**, with a noteworthy feature that the hydrated form, **6a**, obtained from CH_3OH is isomorphous with the reported structure (**PELMUR**) of its analog, *bpyee*. Since, the anhydrous form of **PELMUR** is not known so far, crystallization of **CB** and *bpyee* has been further carried out from different solvents to explore the possibly unnoticed anhydrous form. Indeed, such experiments gave crystals of different geometry **7** and **7a** from CH_3CN and C_2H_5OH solutions, respectively, as discussed below.

X-ray diffraction analysis of crystal **7** reveals that it is adorably an anhydrous complex of **CB** and *bpyee* and also shows isomorphism features with that of complex **6**, crystallizing in the same monoclinic space group $P2_1/c$ and similar unit cell dimensions. Apart from that **6** and **7** are also isostructural in terms of $-B(OH)_2$ moiety conformation (*syn–syn*), molecular packing in 2D and 3D arrangements, with the exception of hydrogen bond parameters (distances and angles) as displayed in Fig. S1.† Thus, in **7** also, *homomeric* (O–H···N with H···N, 1.85 Å; O···N, 2.74 Å) and *heteromeric* (O–H···N with H···N, 2.01 Å;

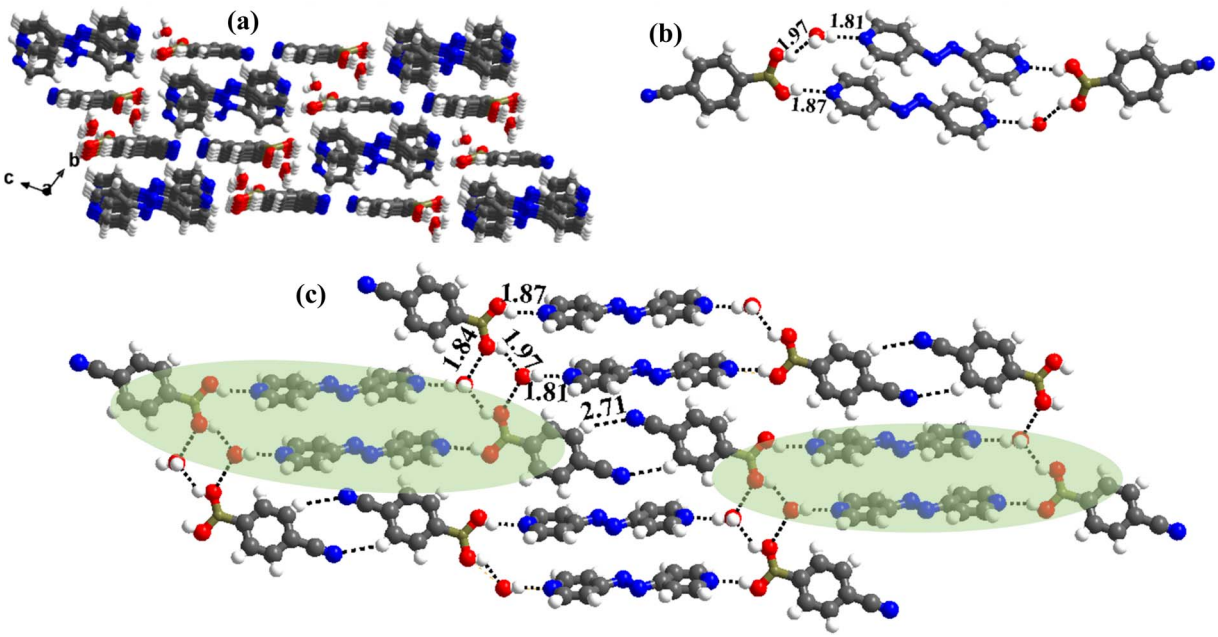

Fig. 7 (a) Three-dimensional stacked layer arrangement in the molecular complex, **6a**. (b) The six-membered cyclic network formed in molecular recognition. (c) Interactions of the hexameric unit in the crystal lattice.

O···N, 2.96 Å, Table 2) hydrogen bonds mediated crisscross ribbon structure is observed.

Molecular complex of CB and *bpyee* in co-crystals of 7a. Crystals of **7a**, obtained by co-crystallization of *bpyee* and **CB** from a C_2H_5OH solution are noted to be dihydrated molecular complexes of the co-formers, as characterized by the single-crystal X-ray diffraction method.

The crystals have an asymmetric unit in a 2 : 1 ratio of the co-formers along with two water molecules, as shown in Table S1,† in the form of an ORTEP drawing. The molecules are arranged in the crystal lattice through the stacking of planar sheets (Fig. 8b), as also observed in the structure of **5**, which has a co-former (*bpyea*), one of the close analogs of *bpyee*; but totally with a different recognition pattern between the co-formers. Furthermore, the structure of **7a** is completely distinct from the other structures (**1–6**) discussed above. In **7a**, the co-formers (**CB** and *bpyee*) do not interact with each other directly through any significant recognition pattern. Thus, the molecules form a host–guest network with the host being **CB** and water molecules with *bpyee* as guest species. In the host network, **CB** molecules form *homomeric* O–H···O hydrogen bonds (H···O, 1.81 Å; O···O, 2.77 Å) in the form of dimers and further interact with water molecules also by O–H···O hydrogen bonds (H···O, 1.84 Å; O···O, 2.71 Å) as depicted in Fig. 8a. The guest moieties (*bpyee*) interact with the host lattice through a series of hydrogen bonds; O–H···N (H···N, 1.79 Å; O···N, 2.71 Å) with water molecules and with **CB** molecules by C–H···O as well as C–H···N hydrogen bonds, as shown in Fig. 8c.

Molecular complexes, 6b and 7b, formed by 4-cyanophenylboronic monoester with *azopy* and *bpyee* co-formers. The needle-shaped crystals obtained concomitantly along with **6a** discussed above, however, are found to be, interestingly, showing an asymmetric unit comprising of *azopy* and *in situ* transformed monoester of **CB** (labeled as **6b**).

The crystals of **6b** crystallize in a monoclinic $P2_1/c$ space group (Table 1), with the asymmetric units having the co-formers (monoester of **CB** and *azopy*) in a 2 : 1 ratio. The constituents are shown in Table S1,† in the form of ORTEP.

The crystal structure analyses of **6b** further illustrate that the recognition moiety between the constituents is a three-component unit, with two O–H···N (H···N, 1.87 Å; O···N, 2.75 Å) hydrogen bonds with each *azopy* molecule glued to two molecules of monoester of **CB**. Because methylation destroys the symmetry of $-B(OH)_2$, the observed conformation of $B(OH)(OCH_3)$ may be regarded as *anti* with respect to the position of $-OCH_3$ and –OH groups. Thus, interaction is established through the participation of *anti*-H-atom and the recognition pattern is shown in Fig. 9a.

Further, from the packing analysis, the arrangement of the molecules in the crystal lattice is in the form of stacked sheets, being separated at a distance of 3.4 Å. A typical arrangement of such a stacked sheet structure is shown in Fig. 9b. Within a typical sheet, the tri-components described above are held together through C–H···O (H···O, 2.42 Å; C···O, 3.47 Å) and C–H···N (H···N, 2.56 Å; C···N, 3.47 Å) hydrogen bonds formed by $-OCH_3$ and –CN groups with hydrogen atoms of *azopy* molecules (Fig. 9c).

Since **6b** was obtained as a concomitant form together with a hydrated form **6a**, co-crystallization of **CB** with *bpyee* has also been repeated from a CH_3OH solution to evaluate if any concomitant crystals were missed out earlier, as only the hydrated form was reported in the literature from such

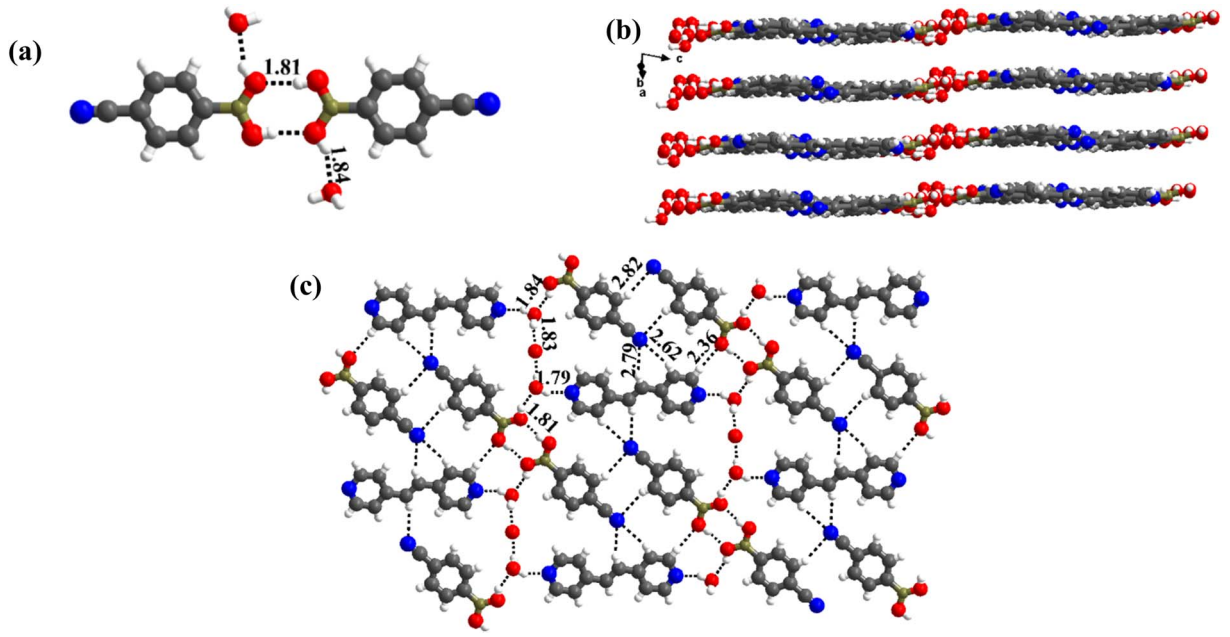

Fig. 8 (a) Basic recognition of CB with *bpyee* in hydrated complex 7a. (b) Planar-sheet arrangement of the molecules in the crystal lattice. (c) Two-dimensional host–guest network.

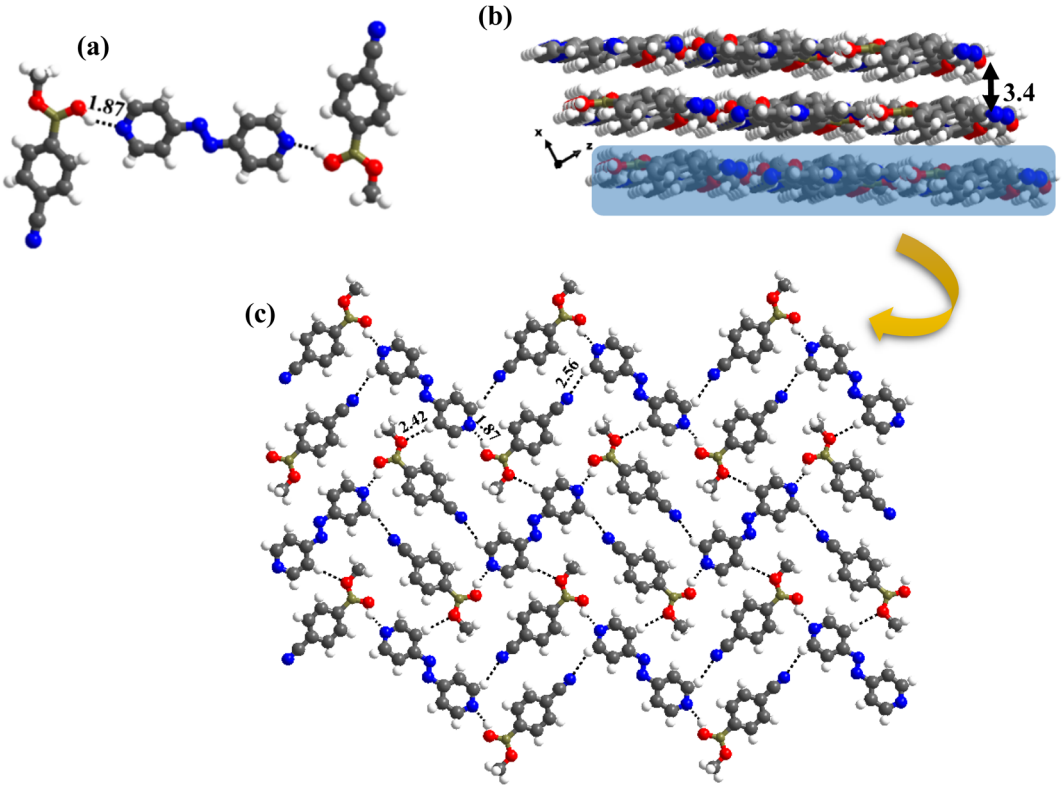

Fig. 9 (a) Molecular recognition observed in the monoester with *azopy*. (b) Stacked sheet arrangement found in the molecular complex **6b**, separated by 3.4 Å. (c) Two-dimensional arrangement of the molecules in the crystal lattice, **6b**.

crystallization experiment. The experiment reveals that this is indeed, the case with the observation of concomitant crystals of different morphologies.

Upon characterization by single-crystal X-ray diffraction, one of the forms was found to be reported hydrated structure (**PELMUR**), while, the other one being with an asymmetric unit comprising of *in situ* transformed monoester of **CB** and *bpyee* (labeled as **7b**), as observed in **6b**. Further, **7b** is also noted to be isomorphous and isostructural **6b**, as both crystallize in the same space group $P2_1/c$ and with similar unit cell parameters (Table 1), as well as similar structural arrangement in the crystal lattices except for hydrogen bond distances and angles. The arrangement of molecules in **7b** is placed in Fig. S2.†

It should be noted that crystals of **1–5**, were also obtained from CH_3OH; but no methylation of **CB** was observed. Such a transformation may be described, as shown in Scheme 2, in terms of the loss of a water molecule from **CB** molecules, in the vicinity of either *azopy*/*bpyee*, which is generally a rare transformation in the co-crystallization process, but otherwise mostly found in the covalent synthesis of base-catalyzed methanolysis reactions.[24]

Based on the single-crystal X-ray diffraction data obtained from a single-crystal of the samples, it is evident that the **CB** molecule forms various exotic supramolecular assemblies with all N-donor molecules. So, in order to ensure the homogeneity of the bulk product, Powder X-Ray Diffraction (PXRD) analysis was conducted on the ground samples of the crystals obtained through solution growth. The result of the analysis demonstrates that the simulated PXRD patterns are corroborated with the experimental patterns, providing confirmation of the exclusive formation of the desired products, as depicted in Section S3.†

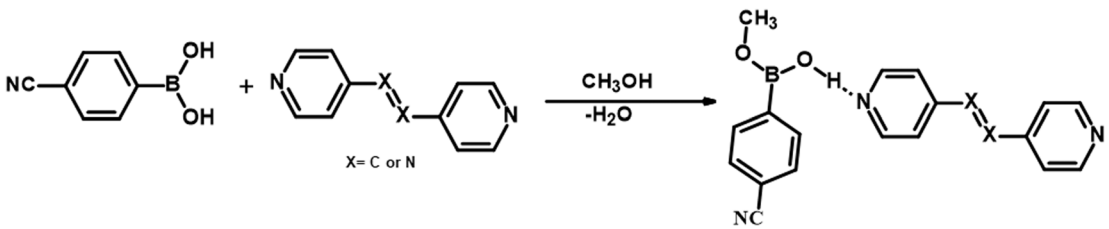

Scheme 2

4. Correlation of structural features and intermolecular interactions energy

4.1. Structural features

Isostructurality and isomorphism. Isostructurality and isomorphism are important phenomena in solid-state structural studies to establish correlations among a series of related structures.[25] Isostructurality vows to similar crystal structures or 3D packing arrangements while isomorphism refers to crystal structures having similar unit cell parameters as well as space groups. Thus, isomorphic crystals often show isostructurality also but not *vice versa*. Isostructurality is more common in multicomponent systems like co-crystals, molecular complexes, solvent inclusion compounds, *etc.*[26] The isostructurality of multicomponent systems can be established using structural index parameters *i.e.*, isostructurality index (Is), unit-cell similarity index ($\prod$), and Xpac dissimilarity index (χ).[27] Is is calculated in the current study, using *Mercury software* (version 3.10.8), by comparing the packing similarity between the pairs in terms of the root-mean-square distance (RMSD) and the degree of similarity between the simulated PXRD patterns of each pair. Mathematical expressions of these calculations are described in Section S4.†

The calculated Is, $\prod$, RMSD, PXRD similarity and χ for all co-crystal pairs are listed in Table S2.† Among all structures, co-crystal pairs **6**/7 and **6b**/**7b** show the highest Is values 97.5 and 97.0%, respectively, as both the pairs are isomorphous as listed in Table 3. However, the hydrated structures of *azopy* (**6a**) and *bpyea* (**5**) as well as each of them along with the reported hydrated structure of *bpyee*, show similar Is values (~65–70%) as observed in **6**/7 and **6b**/**7b**, but the $\prod$ values diverge more (Table 3), which may be due the difference in packing arrangement observed in these crystal lattices.

Table 3 Details of isostructural and isomorphous analysis for the co-crystal pairs

Co-crystals pair	$\prod$	Is (%)	RMSD	PXRD	χ
6/7	0.011	97.5	0.025	0.959	3.2
6b/**7b**	0.015	97.0	0.03	0.932	2.2
6a/**PELMUR**	0.008	72.7	0.273	0.986	2.6
5/**PELMUR**[a]	0.0179	64.3	0.357	0.922	—
6a/**5**	0.0267	65.5	0.345	0.924	—

[a] **PELMUR**, ref code for the reported **CB** and *bpyee* hydrated co-crystal.

The Xpac analysis, computing dissimilarity index (χ), reinforces the observed isostructural features. Herein the points (δ_a, δ_p) are closer to the origin in the structures of **6**/7, **6b**/**7b**, and **6a**/**PELMUR** pairs, suggesting a stronger correlation. In each of these examples, the observed Xpac dissimilarity index (χ = 3.2, 2.2 and 2.6), is shown in the right corner of Fig. 10.

A comparison of experimental and computed (BFDH) morphology. Using a Leica optical microscope, equipped with a stereo zoom camera, images of the crystals are recorded for structures, **1**–**7**, **6a**, **6b**, **7a** and **7b**, which are displayed in Fig. 11. The images primarily refer to four shapes, needles, blocks, plates and a blade. The needles are observed in the structures of **1**, **2**, **6b**, **7a** and **7b**, while blocks are found to be in complexes **4** and **6a**. Further, crystals **3**, **6** and **7** exhibit plate morphology and molecular complex **5** forms blade shape crystals, a standalone geometry among all the complexes.

Shapes of crystals, referred to as morphology, in general, indeed will be the reflection of the packing (arrangement) of molecules in crystal lattices. But, depending upon the growth conditions, often the experimental shapes of the crystals do not always truly corroborate with the observed arrangement of molecules deduced from the structural evaluation carried out by single-crystal X-ray diffraction. Thus, several computational evaluation methods are developed to understand the true morphology of the crystals and thereby compare them with the experimental observations to authenticate the real shapes of the crystals.

Among the available different methodologies and procedures, morphology prediction modules available within *Mercury software*,[28] Bravais–Friedel–Donnay–Harker (BFDH) morphologies, are widely populated to establish a correlation between the experimental and predicted shapes, mainly based on the evaluation of the packing of the molecules.[29]

To assess the observed morphology correlating with the packing patterns, BFDH morphologies are generated considering attachment energy (AE), as listed in Table S3,† and BFDH

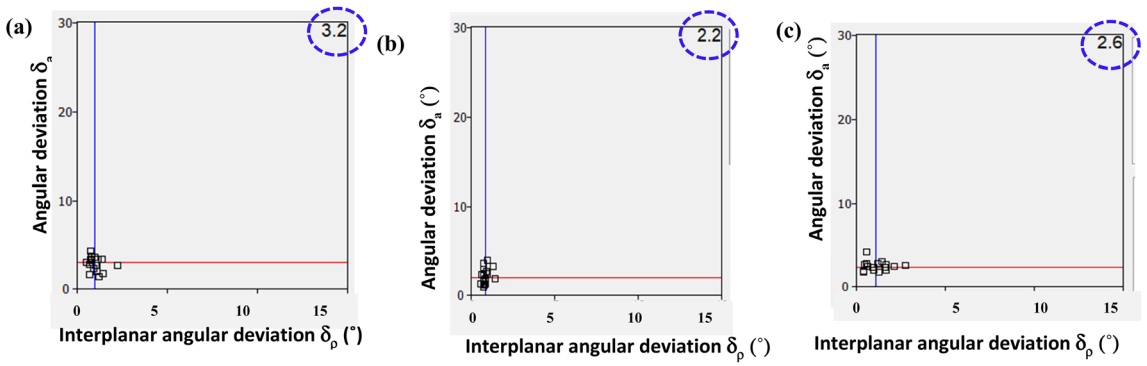

Fig. 10 XPac plot of interplanar angular deviation *vs.* angular deviation (°) for the pair of (a) **6**/7, (b) **6b**/**7b** and (c) **6a**/**PELMUR** illustrating the degree of similarity (top right corner value indicates dissimilarity index).

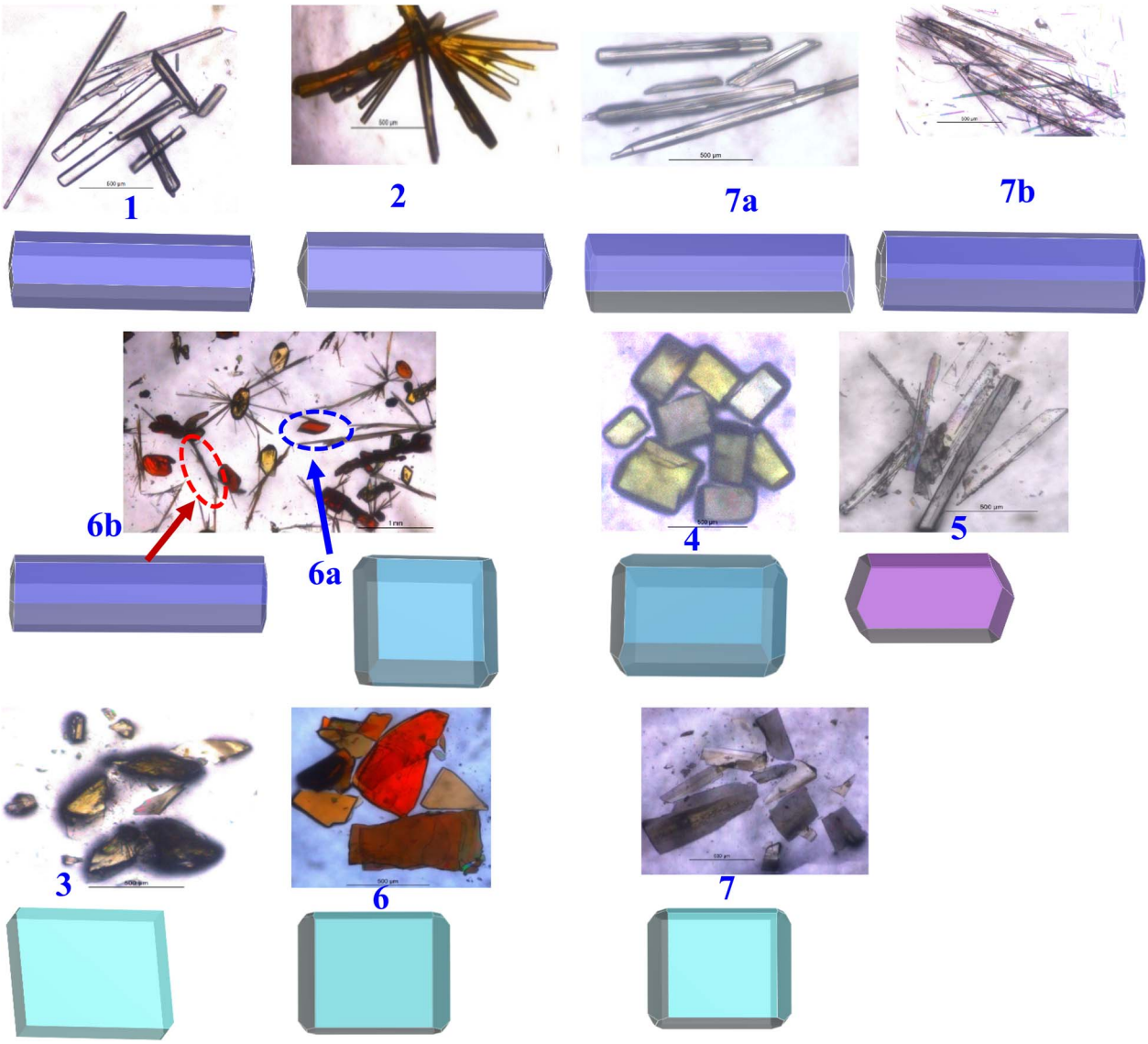

Fig. 11 Presentation of experimental shapes (top) and computed BFDH morphology (bottom) for each structure.

models. The evolved geometries for all crystals are compiled in Fig. 11, which also shows the experimental geometry of the crystals. It is apparent that experimental and computed morphologies show a high degree of overlap, grouping into four types – blocks, needles, plates, and a blade, as observed experimentally also.

4.2. Energy of intermolecular interactions

Intermolecular interactions with gradient energy direct the course of the packing of molecules in crystal lattices. X-ray diffraction data not only assess the determination of positions of the atoms in the lattices but also facilitates the estimation of different characteristics of intermolecular interactions quantitatively in terms of bond distances, angles, *etc.*, that enable further estimate the stability factors like packing coefficients, lattice energy, intermolecular interactions energy, *etc.* In general, as numerous interactions are present in any crystal structure and assessment to establish the correlation between structures is tedious following truly numerical parameters, which leads to the evolution of different types of pictorial representation of strength and energy patterns. Among, Hirshfeld analysis gives a presentation of quantification of the strength of each type of intermolecular interaction through d_{norm} and 2D-finger plots, while 'Energy Frameworks' project total energy evaluating contributions from each interaction as represented by gradient cylinders. Thus, energy calculations have been carried out on all structures **1–7**, **6a**, **6b**, **7a** and **7b** using Crystal Explorer which is embedded with routines/algorithms to carry out Hirshfeld and energy frameworks.

Hirshfeld surface area analysis for the co-crystals. In order to thoroughly understand the strength and role of hydrogen bonds and other intermolecular contacts, as well as to estimate their importance for crystal lattice stability in all the crystals described above, **1–7**, **6a**, **6b**, **7a** and **7b**, Hirshfeld surface

analysis has been carried out by using Crystal Explorer.[19] The Hirshfeld surfaces, mapped with d_{norm}, and corresponding 2D fingerprint plots, clearly summarize quantitatively the nature and types of all the intermolecular interactions experienced by the molecule in the crystal lattices.

In the following section the details of d_{norm} and corresponding 2D fingerprint plots of each co-crystal, **1–7**, **6a**, **6b**, **7a** and **7b**, are shown in Fig. 12, wherein each structure shows a unique Hirshfeld surface and 2D fingerprint plots (details of analysis given in Tables S4 and S5†). The intensity of the surface is determined based on the strength of intermolecular interactions in different color codes and intensities. Thus, deep bright red on the surface at respective donor and acceptor atoms indicates the presence of strong O–H···O or O–H···N interactions; C–H···O appears as a faint red spot and furthermore, white and blue regions on the surface determine the moderate to very weak interactions. Hence, herein Hirshfeld surface of **CB** has been generated to investigate the influence of different N-donors with varied backbones in overall packing in the crystals (Fig. 12).

Analysis of d_{norm} plots shows differently shaded regions in the proximity of N-donor molecules reflecting hydrogen-bonded

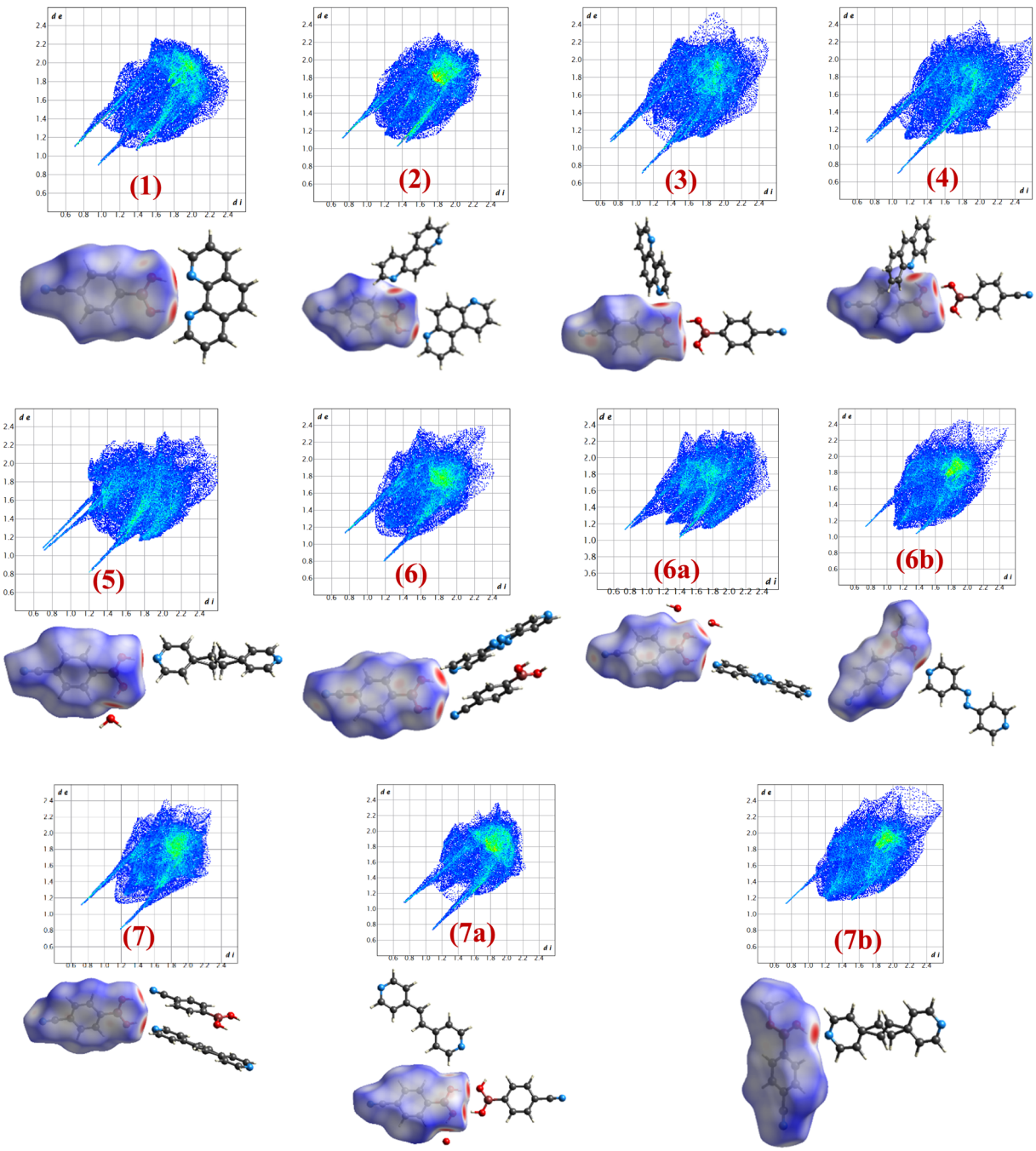

Fig. 12 Hirshfeld surfaces and 2D fingerprint plots of **1–7**, **6a**, **6b**, **7a** and **7b**.

molecular recognition patterns, either *homomeric*/*heteromeric* or both together. For example, structures **1**, **2**, **5**, **6a**, **6b** and **7b** show only *heteromeric* while in structures **3** and **4** both *homomeric* as well as *heteromeric* could be visualized; however, in **7a** only *homomeric* interaction is apparent as the *heteromeric* interaction appears faintly shaded, thus confirming the standalone nature of **7a**. Also, the isostructural pairs (**6**/**7** and **6b**/**7b**) show similar Hirshfeld surface and 2D fingerprint plots.

From 2D fingerprint analysis it is accentuated that in almost all the cases except **6b** and **7b** (crystals with monoester form of **CB**), two prominent long spikes at $d_e + d_i \approx 1.8$ Å, which represent the H···O/O···H or H···N/N···H interactions, with the close contacts range for H···O (10–24%) and H···N (18–25%), as details are shown in Fig. 13. However, **6b** and **7b** show only one spike which is due to the –OH group of monoesters **CB**.

Further, the finger plots disclose that all crystal structures herein follow the general packing features observed in other hydrogen-bonded structures with variable contributions from different intermolecular interactions. Thus, it is apparent from Fig. 13 that all structures show the approximately equal contribution of strong hydrogen bonds (~30%) and secondary hydrogen bonds about 20% with an overall van der Waals of ~30%. In each fingerprint plot, the van der Waals interactions are represented by light to intense green spots at around 3.4 Å, which is due to the C–C interaction or often referred to as π–π interaction.

Energy framework. Energy frameworks are generated intuitively using cylinders to represent connectivity between the centroids of molecular pairs that are held together by intermolecular interactions. Such plots are so informative to explore the energy contributions of different types of interactions towards the overall stability of the crystals with the aid of cylinders of gradient radius that is proportional to the strength of the interaction energy.[30]

This approach has proven to be particularly useful in the study of molecular crystals, where the nature and strength of intermolecular interactions can have a significant impact on the properties and behaviour of the crystals. For example, the utilization of energy frameworks has proven to be valuable in establishing structure–property relationships in molecular crystals, including the study of mechanical behaviour, such as bending, shearing and brittleness of molecular crystals.[31] The basic frameworks are represented as electrostatic energy (E_{ele}, red cylinders), dispersion energy (E_{dis}, green cylinders) and total energy (E_{tot}, blue cylinders).

Therefore, energy frameworks are developed to analyze and comprehend the diverse crystals packing of co-crystals **1**–**7**, **6a**, **6b**, **7a** and **7b**, by generating overlapped energy frameworks onto the packing plots, as represented in Fig. 14, for selected structures (**1**, **5**, **6**, **7** and **7a**) while the same was shown for all the structures in Table S5.†

Analysis of all the plots reveals that electrostatic interactions play a pivotal role in the crystal packing compared to dispersive forces as the radius of green cylinders is so low compared to red ones, except in structure **7a**. A close look at the electrostatic interactions reveals that in structure **1**, the high thickness of the cylinders compared to other structures with high stabilization energy (−93.1 kJ mol^{-1}) indeed reflects the significance of distinct dual *heteromeric* O–H···N hydrogen bonds, among all structures in this study, being facilitated by juxtaposed N-atoms on *110phen*. Similar features are also observed in structure **5** (hydrated **CB** and *bpyea*).

Further, a striking feature is that in structure **7a**, dispersion energy is prominent over electrostatic (Fig. 14), as clearly visible with thick green cylinders, which is indeed in agreement with the structural features in **7a** as the *heteromeric* interactions are obsolete in the form of only weak interactions like C–H···N and C–H···O hydrogen bonds. In fact, the representation authenticates the observation of standalone structure (host–guest type) features of **7a**, in this series as discussed in the corresponding structural description above. A noteworthy observation that could be deduced is that *homomeric* interactions between **CB** molecules despite being in the category of strong hydrogen bonds (O–H···O) could contribute only a little towards the total energy of the crystal lattice.

In general, *heteromeric* interactions are known to be stronger than *homomeric* interactions. In fact, the same is reinforced with the energy terms observed in structures **3** and **4** (Table S5†),

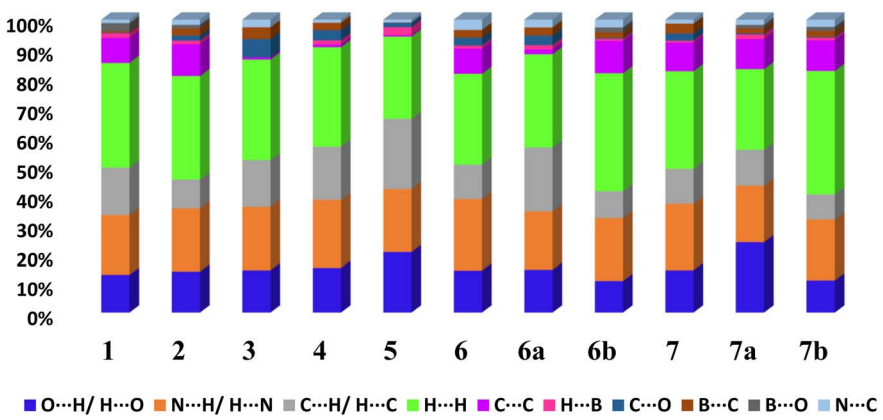

Fig. 13 The relative contribution of different types of intermolecular interactions in crystal lattices considering CB as a dominant surface 1–7, 6a, 6b, 7a and 7b.

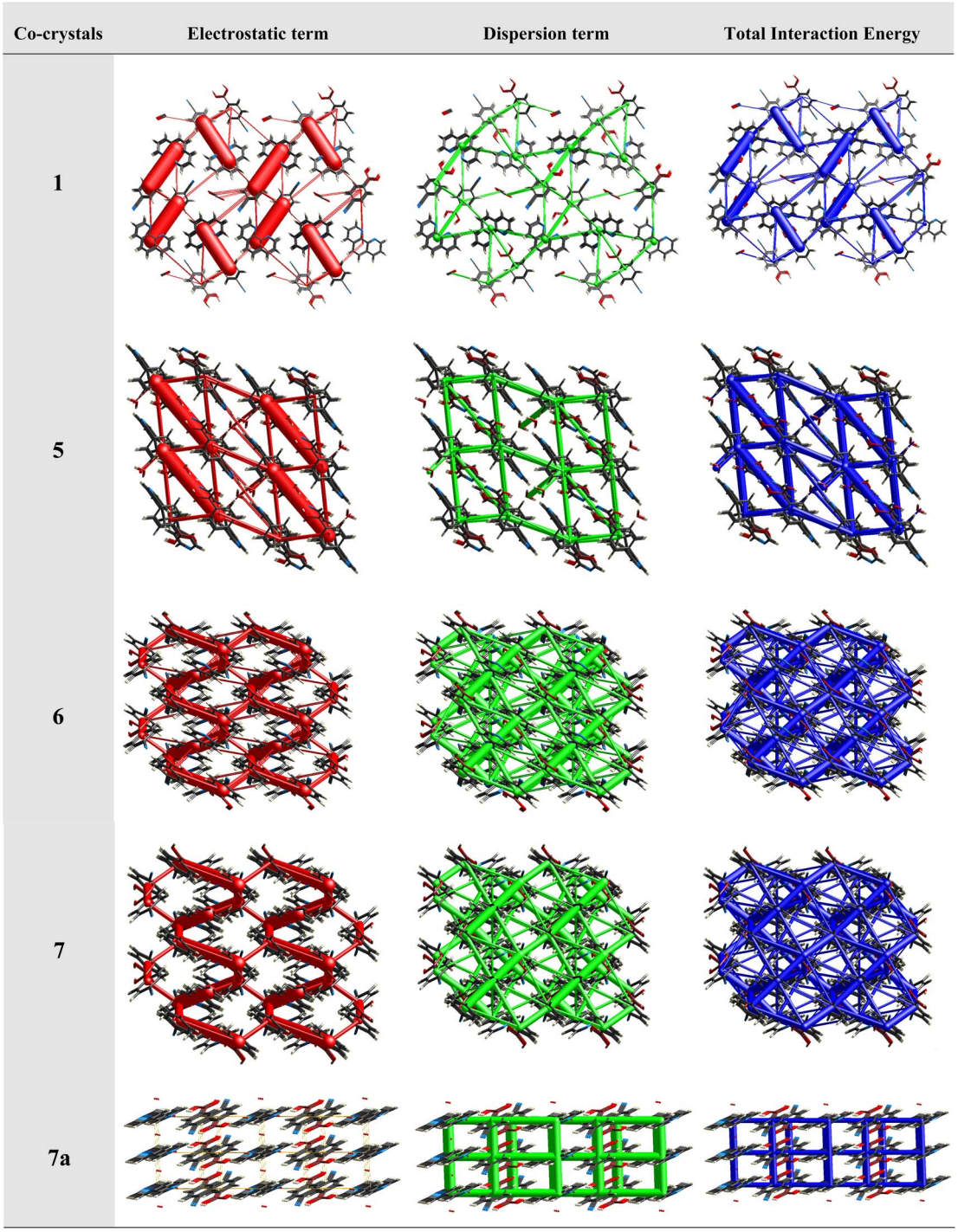

Fig. 14 Pictorial representation of the energy frameworks for some selected co-crystals.

wherein both form *homomeric* and *heteromeric* interactions simultaneously, as *heteromeric* O–H···N hydrogen bonds show higher energy −46.3 and −48.9 kJ mol^{-1} compared to the *homomeric* O–H···O hydrogen bonds, which are at −43.6 and −42.8 kJ mol^{-1}, respectively for **3** and **4**.

In addition, the isostructural features are well reflected with the energy frameworks showing similar energy gradients in the structures **6**/**7** and **6b**/**7b** (see Fig. 14). However, in all other structures, the contributions towards total energy are through the equal competence of electrostatic and dispersive energy, as represented in ESI (Table S5†).

5. Conclusions

Some supramolecular assemblies of **CB** with different N-donor compounds, distinguished by geometrical flexibility have been discussed highlighting the significance of –B(OH)$_2$ moiety for its ability to form a variety of complexes, particularly due to the

conformational flexibility that leads to the formation of hydrogen bonds in topologically different patterns. Though a majority of the complexes $-B(OH)_2$ show a *syn–anti* conformation, the formation of *syn–syn* noted in some complexes indeed strengthens its prevalence, especially in the presence of N-donors with juxtaposed N-atoms, for instance, *110phen* compared to analogous *14-* and *17phen*. Also, observation of different complexes with the same co-formers particularly in the form of hydrates and anhydrous further signifies the importance of multiple crystallization experiments by varying solvents of crystallization, specifically with linear N-donor ligands. Furthermore, the study highlights the *in situ* covalent bond formation with ease, being influenced by selective co-formers that possess reactive functionality. Thus, **CB** undergoes monoester transformation in the co-crystallization studies with N-donors *bpyee* and *azopy* that have C=C and N=N, respectively, while it remains intact in the presence of *bpyea* (an analog of *bpyee* and *azopy*), which has saturated $(-CH_2-)_2$ moiety only. The observed structural features are well corroborated through computational methods and also by calculating isostructurality, evaluation of the strength of intermolecular interactions (Hirshfeld surface analysis) and energy frameworks using Crystal Explorer. Furthermore, experimentally observed morphology of the crystals in the form of needles, blocks, plates and a blade are validated by performing BFDH morphology calculations using Mercury.

Abbreviations

CB	Cyanophenylboronic acid
110phen	1,10-Phenanthroline
47phen	4,7-Phenanthroline
17phen	1,7-Phenanthroline
acr	Acridine
bpyea	1,2-Bis(4-pyridyl)ethane
bpyee	1,2-Bis(4-pyridyl)ethene
azopy	4,4′-Azopyridine

Conflicts of interest

The authors declare no conflict of interest.

Acknowledgements

We acknowledge IIT Bhubaneswar for infrastructure and DST-SERB, New Delhi, for the financial support.

References

1 (*a*) J. C. MacDonald and G. M. Whitesides, *Chem. Rev.*, 1994, **94**, 2383–2420; (*b*) D. Braga and F. Grepioni, *Crystal Engineering: from Molecules and Crystals to Materials*, Springer, 1999; (*c*) P. Alivisatos, P. F. Barbara, A. W. Castleman, J. Chang, D. A. Dixon, M. L. Klein, G. L. McLendon, J. S. Miller, M. A. Ratner and P. J. Rossky, *Adv. Mater.*, 1998, **10**, 1297–1336; (*d*) J. L. Atwood, *Comprehensive Supramolecular Chemistry II*, Elsevier, 2017.

2 (*a*) G. R. Desiraju, *Nature*, 2001, **412**, 397–400; (*b*) L. Sun, W. Zhu, X. Zhang, L. Li, H. Dong and W. Hu, *J. Am. Chem. Soc.*, 2021, **143**, 19243–19256; (*c*) D. Braga and F. Grepioni, *Acc. Chem. Res.*, 2000, **33**, 601–608; (*d*) J. Bernstein, J. J. Novoa, R. Boese and S. A. Cirkel, *Chem.–Eur. J.*, 2010, **16**, 9047–9055; (*e*) S. Ahn, J. PrakashaReddy, B. M. Kariuki, S. Chatterjee, A. Ranganathan, V. R. Pedireddi, C. N. R. Rao and K. D. M. Harris, *Chem.–Eur. J.*, 2005, **11**, 2433–2439.

3 (*a*) G. R. Desiraju, *Angew. Chem., Int. Ed.*, 2007, **46**, 8342–8356; (*b*) S. Subramanian and M. J. Zaworotko, *Coord. Chem. Rev.*, 1994, **137**, 357–401; (*c*) Q. Huang, W. Li, Z. Mao, L. Qu, Y. Li, H. Zhang, T. Yu, Z. Yang, J. Zhao and Y. Zhang, *Nat. Commun.*, 2019, **10**, 3074.

4 (*a*) P. Li, M. R. Ryder and J. F. Stoddart, *Acc. Mater. Res.*, 2020, **1**, 77–87; (*b*) K. S. Eccles, R. E. Morrison, A. R. Maguire and S. E. Lawrence, *Cryst. Growth Des.*, 2014, **14**, 2753–2762; (*c*) S. Easmin and V. R. Pedireddi, *Cryst. Growth Des.*, 2023, **23**, 2802–2811.

5 (*a*) P. S. Pereira Silva, R. A. E. Castro, E. Melro, M. R. Silva, T. M. R. Maria, J. Canotilho and M. E. S. Eusébio, *J. Therm. Anal. Calorim.*, 2015, **120**, 667–677; (*b*) M. Nowak, A. J. Dyba, J. Janczak, A. Morritt, L. Fábián, B. Karolewicz, Y. Z. Khimyak, D. E. Braun and K. P. Nartowski, *Mol. Pharm.*, 2022, **19**, 456–471.

6 (*a*) I. Georgiou, S. Kervyn, A. Rossignon, F. De Leo, J. Wouters, G. Bruylants and D. Bonifazi, *J. Am. Chem. Soc.*, 2017, **139**, 2710–2727; (*b*) M. R. Shimpi, N. SeethaLekshmi and V. R. Pedireddi, *Cryst. Growth Des.*, 2007, **7**, 1958–1963; (*c*) S. Forensi, A. Stopin, F. de Leo, J. Wouters and D. Bonifazi, *Tetrahedron*, 2020, **76**, 131299; (*d*) S. Varughese, S. B. Sinha and G. R. Desiraju, *Sci. China: Chem.*, 2011, **54**, 1909–1919.

7 (*a*) N. Miyaura and A. Suzuki, *Chem. Rev.*, 1995, **95**, 2457–2483; (*b*) D. J. Wallace and C.-y. Chen, *Tetrahedron Lett.*, 2002, **43**, 6987–6990; (*c*) A. N. Cammidge and K. V. Crépy, *Chem. Commun.*, 2000, 1723–1724.

8 (*a*) J. N. Cambre and B. S. Sumerlin, *Polymer*, 2011, **52**, 4631–4643; (*b*) B. Wang, K. Yoshida, K. Sato and J.-i. Anzai, *Polymers*, 2017, **9**, 202.

9 (*a*) G. T. Williams, J. L. Kedge and J. S. Fossey, *ACS Sens.*, 2021, **6**, 1508–1528; (*b*) T. D. James, K. S. Sandanayake and S. Shinkai, *Angew. Chem., Int. Ed.*, 1996, **35**, 1910–1922.

10 (*a*) W. Yang, X. Gao and B. Wang, *Med. Res. Rev.*, 2003, **23**, 346–368; (*b*) B. Muz, A. K. Azab, L. Confalonieri, E. Del Grosso, S. Fallarini, D. Imperio and L. Panza, *Bioorg. Med. Chem.*, 2022, **59**, 116659.

11 (*a*) S.-T. Yang, J. Kim, H.-Y. Cho, S. Kim and W.-S. Ahn, *RSC Adv.*, 2012, **2**, 10179–10181; (*b*) Y. Kubo, R. Nishiyabu and T. D. James, *Chem. Commun.*, 2015, **51**, 2005–2020; (*c*) S. D. Brucks, D. N. Bunck and W. R. Dichtel, *Polymer*, 2014, **55**, 330–334.

12 (*a*) V. R. Pedireddi and N. SeethaLekshmi, *Tetrahedron Lett.*, 2004, **45**, 1903–1906; (*b*) M. Talwelkar and V. R. Pedireddi, *Tetrahedron Lett.*, 2010, **51**, 6901–6905; (*c*) J. J. Campos-Gaxiola, B. A. García-Grajeda, I. F. Hernández-Ahuactzi, J. A. Guerrero-Álvarez, H. Höpfl and A. Cruz-Enríquez,

CrystEngComm, 2017, **19**, 3760–3775; (*d*) P. Tomaszewski, M. Wiszniewski, J. Serwatowski, K. Woźniak, K. Durka and S. Luliński, *Dalton Trans.*, 2018, **47**, 16627–16637.

13 (*a*) S. Weinstein, L. Leiserowitz and E. Gil-Av, *J. Am. Chem. Soc.*, 1980, **102**, 2768–2772; (*b*) A. D. Burrows, *Supramolecular Assembly via Hydrogen Bonds I*, 2004, pp. 55–96; (*c*) N. Shan, A. Bond and W. Jones, *Cryst. Eng.*, 2002, **5**, 9–24.

14 (*a*) D. G. Hall, *Boronic Acids: Preparation, Applications in Organic Synthesis and Medicine*, John Wiley & Sons, 2006; (*b*) D. G. Hall, *Boronic acids: Preparation and Applications in Organic Synthesis and Medicine* 2005, pp. 1–99; (*c*) N. Fujita, S. Shinkai and T. D. James, *Chem.–Asian J.*, 2008, **3**, 1076–1091; (*d*) T. D. James, *Beilstein J. Org. Chem.*, 2016, **12**, 391–405; (*e*) R. Nishiyabu, Y. Kubo, T. D. James and J. S. Fossey, *Chem. Commun.*, 2011, **47**, 1124–1150.

15 M. TalwelkarShimpi, S. Öberg, L. Giri and V. R. Pedireddi, *Cryst. Growth Des.*, 2017, **17**, 6247–6254.

16 G. Sheldrick, *Acta Crystallogr., Sect. A: Found. Adv.*, 2014, **70**, C1437.

17 A. Spek, *J. Appl. Crystallogr.*, 2003, **36**, 7–13.

18 G. Bergerhoff, M. Berndt and K. Brandenburg, *J. Res. Natl. Inst. Stand. Technol.*, 1996, **101**, 221.

19 P. R. Spackman, M. J. Turner, J. J. McKinnon, S. K. Wolff, D. J. Grimwood, D. Jayatilaka and M. A. Spackman, *J. Appl. Crystallogr.*, 2021, **54**, 1006–1011.

20 (*a*) M. Talwelkar and V. Pedireddi, *Tetrahedron Lett.*, 2010, **51**, 6901–6905; (*b*) S. SeethaLekshmi, S. Varughese, L. Giri and V. Pedireddi, *Cryst. Growth Des.*, 2014, **14**, 4143–4154.

21 S. Saha and G. R. Desiraju, *J. Am. Chem. Soc.*, 2018, **140**, 6361–6373.

22 J. PrakashaReddy and V. R. Pedireddi, *Tetrahedron*, 2004, **60**, 8817–8827.

23 (*a*) V. Nagarajan, M. R. Shimpi and V. R. Pedireddi, *J. Mol. Struct.*, 2013, **1050**, 216–221; (*b*) K. Fucke, S. A. Myz, T. P. Shakhtshneider, E. V. Boldyreva and U. J. Griesser, *New J. Chem.*, 2012, **36**, 1969–1977.

24 (*a*) I. B. Banković-Ilić, Z. B. Todorović, J. M. Avramović, A. V. Veličković and V. B. Veljković, *Fuel Process. Technol.*, 2015, **137**, 339–350; (*b*) H. Liu, J. Chen, L. Chen, Y. Xu, X. Guo and D. Fang, *ACS Sustainable Chem. Eng.*, 2016, **4**, 3140–3150.

25 S. Ranjan, R. Devarapalli, S. Kundu, S. Saha, S. Deolka, V. R. Vangala and C. M. Reddy, *IUCrJ*, 2020, **7**, 173–183.

26 (*a*) R. Thakuria and A. Nangia, *Cryst. Growth Des.*, 2013, **13**, 3672–3680; (*b*) D. Cinčić, T. Friščić and W. Jones, *New J. Chem.*, 2008, **32**, 1776–1781; (*c*) A. J. Cruz Cabeza, G. M. Day, W. S. Motherwell and W. Jones, *J. Am. Chem. Soc.*, 2006, **128**, 14466–14467.

27 T. Gelbrich and M. B. Hursthouse, *CrystEngComm*, 2006, **8**, 448–460.

28 C. F. Macrae, I. Sovago, S. J. Cottrell, P. T. A. Galek, P. McCabe, E. Pidcock, M. Platings, G. P. Shields, J. S. Stevens, M. Towler and P. A. Wood, *J. Appl. Crystallogr.*, 2020, **53**, 226–235.

29 J. Prywer, *J. Cryst. Growth*, 2004, **270**, 699–710.

30 (*a*) D. Dey, S. Bhandary, S. P. Thomas, M. A. Spackman and D. Chopra, *Phys. Chem. Chem. Phys.*, 2016, **18**, 31811–31820; (*b*) C. F. Mackenzie, P. R. Spackman, D. Jayatilaka and M. A. Spackman, *IUCrJ*, 2017, **4**, 575–587.

31 (*a*) S. P. Thomas, M. W. Shi, G. A. Koutsantonis, D. Jayatilaka, A. J. Edwards and M. A. Spackman, *Angew. Chem., Int. Ed.*, 2017, **56**, 8468–8472; (*b*) M. J. Turner, S. P. Thomas, M. W. Shi, D. Jayatilaka and M. A. Spackman, *Chem. Commun.*, 2015, **51**, 3735–3738; (*c*) M. Ghora, P. Majumdar, M. Anas and S. Varghese, *Chem.–Eur. J.*, 2020, **26**, 14488–14495.